Applied Physics Letters

Readable racetrack memory via ferromagnetically coupled chiral domain walls

Cite as: Appl. Phys. Lett. **113**, 152401 (2018); https://doi.org/10.1063/1.5049859
Submitted: 26 July 2018 • Accepted: 21 September 2018 • Published Online: 08 October 2018

Maokang Shen, Yue Zhang, Long You, et al.

AIP Publishing

Readable racetrack memory via ferromagnetically coupled chiral domain walls

Maokang Shen, Yue Zhang,[a] Long You, and Xiaofei Yang
School of Optical and Electronic Information, Huazhong University of Science and Technology, Wuhan 430074, People's Republic of China

(Received 26 July 2018; accepted 21 September 2018; published online 8 October 2018)

Current-induced motion of domain walls (CIMDWs) with the interfacial Dzyaloshinskii-Moriya interaction (DMI) in heavy metal (HM)/ferromagnetic (FM) metal multilayers has attracted attention owing to their potential applications in novel magnetic memories. In recent years, the CIMDW at ultrahigh speed has been observed in a synthetic antiferromagnetic (SAF) multilayer with a high storage density because of the weak stray field. However, due to the zero net magnetization, the reading of information from the SAF multilayer is still challenging. In this work, we propose a *readable* racetrack memory consisting of a synthetic ferromagnetic multilayer composed of two FM layers with an interlayer FM coupling. One FM layer had an isotropic DMI, while the other had an anisotropic DMI. This difference of DMIs resulted in the opposite tilting directions of the DW planes in the two layers. This tilting was inhibited by a strong interlayer FM coupling, resulting in an increase in the DW velocity and the reduction of the minimum allowed spacing between two adjacent DWs. In addition, the FM coupling enhanced the stray field, and the stored information could be read conveniently using a conventional reading head. Therefore, our proposal paves the way for the fabrication of a racetrack memory with high reading speed, large storage density, and good readability. *Published by AIP Publishing*. https://doi.org/10.1063/1.5049859

Racetrack memories, based on the current induced motion of domain walls (CIMDWs), have attracted attention owing to their potential applications in magnetic memories with high storage density and reading speed and low dissipation.[1,2]

Besides conventional DWs in ferromagnetic (FM) nanowires,[1] special magnetic microstructures, such as skyrmions and DWs with chirality, are observed in a heavy metal (HM)/FM metal multilayer with the interfacial Dzyaloshinskii-Moriya interaction (DMI).[3–9] When a current is injected, skyrmions or chiral DWs are driven at a high speed due to the combined action of spin-orbit torque (SOT) and DMI.[2] However, strong DMI also tilts the plane of a moving DW.[10–13] The neighboring DWs tilt towards opposite directions because of symmetry, and they may be connected at a large tilting angle.[10] As a result, the storage density and the reading speed are limited.

To improve the function of racetrack memory, the coupled racetrack with two or more FM layers was proposed. For the CIMDWs due to STT, Purnama *et al.* reported the depressed Walker breakdown through an interlayer magnetostatic coupling.[14] Recently, an ultrahigh moving speed with inhibited DW tilting was observed for the coupled DWs in a synthetic antiferromagnet (SAF) with interlayer AFM exchange coupling.[2,15–17] On the other hand, the coupled domains offer a negligible stray field due to the zero net magnetization, which enhances the storage density. However, this weak stray field may also increase the difficulty in reading using a reading head that is close to the racetrack.

In this work, we propose a readable racetrack memory with high reading speed and high storage density in a synthetic ferromagnet (SF), two FM layers with an interlayer FM coupling. One FM layer exhibits a conventional isotropic DMI (iDMI), while the other has an anisotropic DMI (aDMI) appearing in materials with special symmetries.[18–20] We found that the tilting of the paired DWs was inhibited under a strong interlayer exchange coupling. As a result, the DW velocity and the minimum spacing between the neighboring DWs in the SF were both greater than that in the single FM layer. Additionally, the strong stray field of the paired DWs also improves the readability by a conventional reading head.

Figure 1 shows a schematic of the HM1/FM1/NM/FM2/HM2 multilayer. NM denotes the normal metal layer acting as a medium for Ruderman–Kittel–Kasuya–Yosida (RKKY)-type FM exchange coupling between FM1 and FM2. The general DMI energy density is expressed as[20,21]

$$\varepsilon_{\mathrm{aDM}} = D_{\mathrm{x}}\left(m_{\mathrm{z}}\frac{\partial m_{\mathrm{x}}}{\partial x} - m_{\mathrm{x}}\frac{\partial m_{\mathrm{z}}}{\partial x}\right) + D_{\mathrm{y}}\left(m_{\mathrm{z}}\frac{\partial m_{\mathrm{y}}}{\partial y} - m_{\mathrm{y}}\frac{\partial m_{\mathrm{z}}}{\partial y}\right), \tag{1}$$

where m_{x}, m_{y}, and m_{z} are the components of unit magnetization. The aDMI is a tensor with different components for different terms of Lifshitz invariants, i.e., $D_{\mathrm{x}} \neq D_{\mathrm{y}}$.[20] The conventional iDMI is represented by a scale (D), that is, $D_{\mathrm{x}} = D_{\mathrm{y}} = D$.

In Fig. 1, HM1/FM1 is the bottom bilayer with aDMI, and FM2/HM2 is the top one with iDMI. The aDMI requires special lattice symmetry, but the iDMI exists in polycrystalline and amorphous bilayer and is tunable by modifying the properties of FM2, HM2, or the FM2/HM2 interface.[20,22] In the simulation, the aDMI tensor of HM1/FM1 was fixed, while the D of FM2/HM2 was varied in the experimentally achievable range.[20,22]

[a]Author to whom correspondence should be addressed: yue-zhang@hust.edu.cn

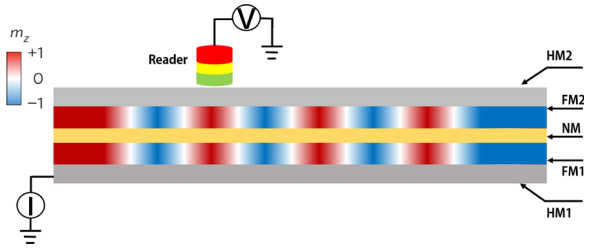

FIG. 1. Schematic of the model for a readable racetrack memory with an FM coupling. The structure is HM1/FM1/NM/FM2/HM2. Here, the bottom HM1/FM1 has an aDMI, while the top FM2/HM2 exhibits an iDMI. The information can be read using a conventional reader to detect the stray field of the paired DWs.

In the multilayer, the D_x of HM1/FM1 and the D of FM2/HM2 need to have the same sign to ensure the same chirality, suitable for the interlayer FM coupling. Under this condition, the spin Hall angles of the two HM layers should be opposite as HM1 is below FM1 and HM2 is above FM2. In this case, the spins flowing into the two FM layers have the same orientation, rotating the moments in the two FM layers towards the same direction. This has been experimentally demonstrated by Krishnia *et al.*[23] However, the DWs in the two FM layers can move together with only one HM layer if only the interlayer exchange coupling is sufficiently strong.[15] Certain combinations of HM/FM multilayers, such as Ru/W/Co and Co/Ru[22] and Pt/Co and Co/Ir/Pt,[20] satisfy the above requirements.

The investigation was performed numerically using the micromagnetic simulation software named the Object-Oriented MicroMagnetic Framework (OOMMF) containing the widely accepted damping-like SOT.[24] (The field-like SOT is considered in the supplementary material.) The code for DMI was expanded to include aDMI. We considered a 100-nm-wide and 2000-nm-long nanotrack. The thickness of each FM layer was 0.6 nm. The dimension of the unit cell was 2 nm (length) × 1 nm (width) × 0.6 nm (thickness). The parameters for the ultra-thin Co film with perpendicular magnetic anisotropy (PMA) were as follows:[21,25] the PMA constant $K = 8 \times 10^5$ J/m^3, the saturation magnetization $M_S = 7 \times 10^5$ A/m, the exchange stiffness constant $A = 1 \times 10^{11}$ J/m, and the spin Hall angle $\theta_{SH} = 0.3$. The DMI constant was varied between -0.05 mJ/m^2 and -2.5 mJ/m^2, an experimentally achievable range.[21,22] The interlayer exchange coupling constant (σ) varies between 0 and 0.1 mJ/m^2, in the range for RKKY exchange coupling.[15,21] σ is also relevant to the interfacial lattice symmetry, yet modifying the thickness of NM in experiments offers the equivalent result. The current density (J) was between 8.3×10^9 A/m^2 and 1.6×10^{11} A/m^2.

The Néel-type static DWs for both aDMI ($D_x = -D_y = -1.5$ mJ/m^2) and iDMI ($D = -1.5$ mJ/m^2) exhibit left-hand chirality in the inner part of the track [Figs. 2(a) and 2(c)]. However, near the boundaries, the moments have small projections in the y-direction due to the DMI-related boundary conditions.[24] The orientation of moments near the track boundary for aDMI is opposite to that for iDMI [the insets of Figs. 2(a) and 2(c)].

After the static DWs were generated, the CIMDWs were simulated. The DWs tilt [Figs. 2(b) and 2(d)] due to the competition between SOT and DMI ($J = 1.3 \times 10^{11}$ A/m^2). The

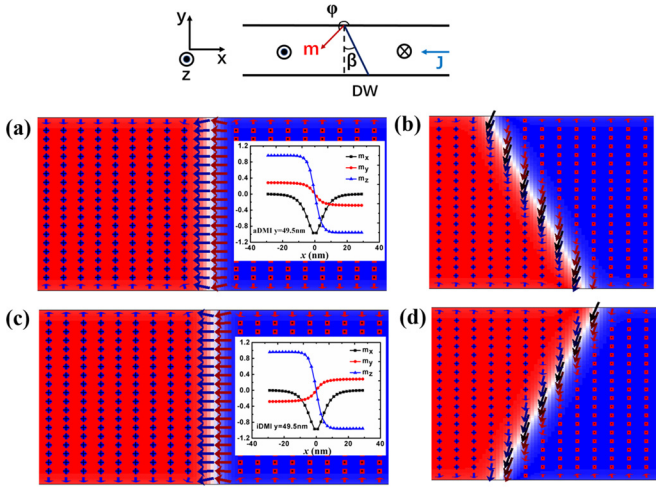

FIG. 2. (a) Structure of the moments in the static DW with aDMI (the inset shows the variation of m_x, m_y, and m_z across the DW near the track boundary). (b) Structure of the moments of a moving DW with aDMI. (c) Structure of the moments in the static DW with iDMI (the inset shows the variation of m_x, m_y, and m_z across the DW near the track boundary). (d) Structure of the moments of a moving DW with iDMI. The upper panel defines the coordinate system, the azimuthal angle of the moments in the central of the DW, and the tilting angle of the DW plane.

damping-like SOT rotates the DW moments, leading to the transition from a chiral Néel DW to a Bloch-like one. On the other hand, the DMI tries to maintain the chiral Néel structure. As a compromise, the DW plane tills at the cost of an increased demagnetization energy.[11] We also noticed that the tilting orientation of the DW with iDMI is opposite to that for aDMI. As $D_x = D_y$ for the iDMI and $D_x = -D_y$ for the aDMI, the y component of iDMI effective field is opposite to that of aDMI. The mechanism for the DMI-relevant DW tilting was also analyzed in more detail using a collective coordinate model (CCM), which is described in the supplementary material.

The SOT-induced motion of the paired DWs in a bilayer composed of two FM-coupled nanotracks was also investigated ($D_x = -1.5$ mJ/m^2 and $J = 1.3 \times 10^{11}$ A/m^2), with $\sigma = 0.06$ mJ/m^2. One of the tracks had iDMI, while the other track had aDMI (Track-F-ia). As a comparison, the DW motion in a single track with iDMI (Track-i) or aDMI (Track-a) and that in an FM-coupled bilayer with iDMI (Track-F-ii) were also simulated [Figs. 3(a)–3(d)].

In Track-i, Track-a, and Track-F-ii, the tilting direction for the DW with iDMI is opposite to that for aDMI. However, in Track-F-ia, the tilting of the paired DW disappears due to strong interlayer FM coupling. Additionally, the velocity of the paired DWs in Track-F-ia is also higher (the average DW velocities in Track-F-ia, Track-i, Track-a, and Track-F-ii are 460 m/s, 394 m/s, 401 m/s, and 388 m/s, respectively).

The motion of the paired DWs in Track-F-ia has been investigated in more detail to determine the optimal parameters [Figs. 3(e)–3(h)]. When the σ increases from 0 to 0.1 mJ/m^2, the velocity of the paired DWs increases and the tilting angles of the two FM layers decrease. When σ is 0.05 mJ/m^2 or larger, the velocity stabilizes, and the DW tilting is completely inhibited [Fig. 3(e)].

When the D for iDMI increases from 0 to -2.5 mJ/m^2 (the D_x for aDMI is fixed at -1.5 mJ/m^2), the DW velocity

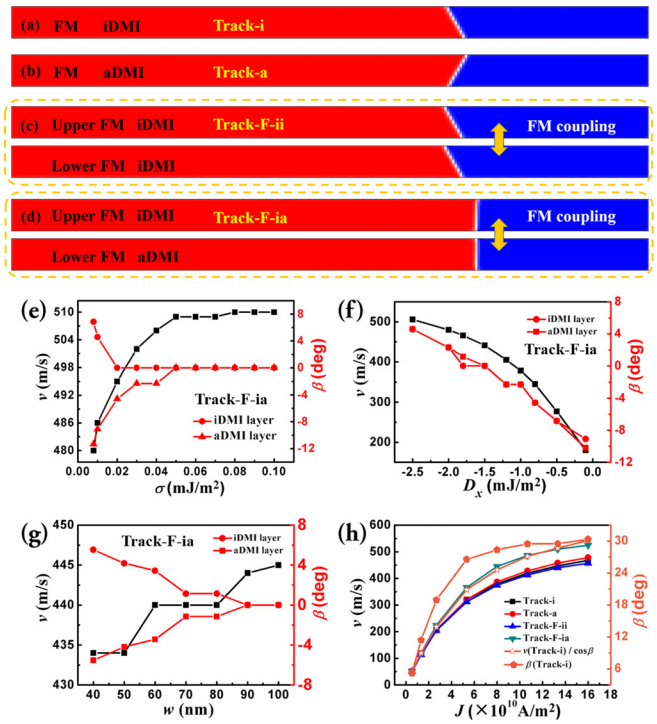

FIG. 3. SOT-induced motion of (a) a DW with iDMI and (b) a DW with aDMI in a single track, (c) the paired DWs with iDMI in an FM-coupled, and (d) the paired DWs in an FM-coupled bilayer (one exhibits iDMI and the other has aDMI). All snapshots were taken when the DWs had been moving for 1 ns. Velocity of the paired DWs and the tilting angles (β) of the DW in the two layers with iDMI and aDMI as a function of (e) the interlayer exchange coupling constant, σ, (f) the D for iDMI, and (g) the track width, w. In (e), D_x of both layers, J, and w is fixed as -1.5 mJ/m^2, 1.3×10^{11} A/m^2, and 100 nm, respectively. In (f), D_x for aDMI is fixed as -1.5 mJ/m^2. J, σ, and w are 8×10^{10} A/m^2, -0.06 mJ/m^2, and 100 nm, respectively. In (g), D_x of both layers, J, and σ is -1.5 mJ/m^2, 8×10^{10} A/m^2, and -0.06 mJ/m^2, respectively. (h) compares the velocity as a function of J in different tracks. D_x of both layers, σ, and w is -1.5 mJ/m^2, -0.06 mJ/m^2, and 100 nm, respectively. β as a function of J is also shown for comparison. It indicates that the velocity of the paired DWs in the FM coupled tracks with different DMIs is related to that in the single FM layer by the cosine of β.

keeps increasing, which is accompanied by the rotation of the DW plane [Fig. 3(f)]. The FM layer with stronger DMI determines the tilting direction of the paired DWs. When the D is identical to the D_x of aDMI, the tilting is completely inhibited.

The track width (w) also affects the velocity and tilting [Fig. 3(g)]. The velocity of the paired DWs increases with the w increasing from 40 nm to 100 nm, which is accompanied by the depressed tilting. Near the track boundary, the moment in one layer cannot be parallel with that in the other layer (Fig. 2), resulting in an unavoidable tilting near the boundary. This boundary effect is significant when w is 60 nm or smaller and becomes negligible when w is 90 nm or greater.

The velocity as a function of J is shown in Fig. 3(h). The DW velocities in Track-i, Track-a, and Track-F-ii are almost the same; however, that in the FM-coupled bilayer with different DMIs is higher. Their difference in the velocity keeps increasing with the increase in J and stabilizes ($\sim$100 m/s) when $J \geq 8 \times 10^{10}$ A/m^2. The velocity of the tilting DW seems to be the projection of the velocity normal to the DW plane in the length direction [Fig. 3(h)]. Therefore, the DW velocity in the track length direction reaches its maximum when the DW plane does not tilt. On the other hand, the tilting angle (β) mainly increases in the low-J region and becomes stable under a large J.[26] Therefore, the difference in the velocity increases mainly at low current densities [Fig. 3(h)].

Besides reading speed, storage density is another important characteristic. To determine the minimum storage density, an array of domains with different spacings between the neighboring DWs was fabricated. In a single FM layer [Fig. 4(a)], the domain spacing was initially set to 80 nm. After the relaxation to generate DWs, the domain spacing was reduced to 78 nm. After the DWs start moving, the DW planes tilt with an average spacing of 78 nm. When the initial domain spacing was smaller, the neighboring DWs were connected because of tilting. However, in the FM-coupled two layers with distinct DMI [Fig. 4(b)], the allowed minimum domain

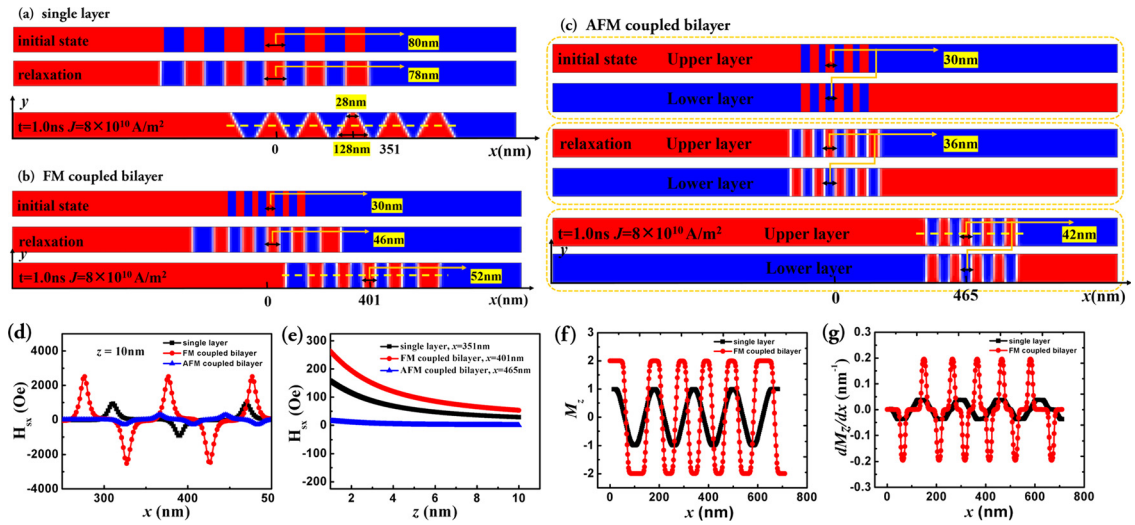

FIG. 4. Minimum allowed DW spacing in the single FM layer with iDMI (a), in the FM coupled two FM layers with different types of DMIs (b), and in the SAF racetrack (c). The stray field in the track length direction (H_{sx}) as a function of x above the DW center at a height of 10 nm (d) and as a function of z above the domain center (e). M_z (f) and the differential of M_z (g) with respect to x for a single FM layer (black dots and lines) and for an FM-coupled bilayer (red dots and lines). The parameters including D_x, σ, and w are -1.5 mJ/m^2, -0.06 mJ/m^2, and 100 nm, respectively.

spacing (l_{dmin}) was 52 nm. Therefore, the inhibition of DW tilting by strong interlayer FM exchange coupling is useful to increase the storage density. The l_{dmin} in the SAF racetrack was even smaller, about 42 nm [Fig. 4(c)].

The l_{dmin} is relevant to the stray field expressed as[27]

$$\frac{H_{sx}}{2M_S} = \ln\left(\frac{z^2+\Delta^2/4}{(h-z)^2+\Delta^2/4}\right) + \frac{4}{\Delta}\left(z\tan^{-1}\frac{\Delta}{2z} - (h-z)\tan^{-1}\frac{\Delta}{2(h-z)}\right). \quad (2)$$

Here, H_{sx}, z, h, and Δ are, respectively, the components of the stray field in the length direction, the z coordinate in the out-of-plane direction, the thickness of the FM layer, and the DW width that is determined by[11,12]

$$\Delta = \sqrt{A/(K-\mu_0 M_s^2/2)}. \quad (3)$$

The H_{sx} above the DW center is the strongest [Fig. 4(d)] and is much weaker above the domain center [Fig. 4(e)]. In both cases, the FM coupled bilayer offers the strongest H_{sx}, while the H_{sx} above the SAF track is the weakest. At a height of several nanometers above the domain center in the upper layer, the H_{sx} of the FM coupled bilayer is around 100 Oe [Fig. 4(e)]. Yet that of the SAF track there is negligible. The weak stray field for the SAF induces both outstanding storage density and difficulty in reading using a conventional reading head that detects the stray field from the domains. Alternatively, the information in the SAF may be labeled by the moment orientation in the upper FM layer, which is determined using an MTJ that is in contact with the racetrack. However, fabricating both the capping layer and MTJ above the upper FM layer is challenging in experiments.

In addition to storage density, in a single FM layer, the DW tilting also causes a gradual change of magnetization from $-M_S$ (M_S) of one domain to M_S ($-M_S$) of the adjacent one. However, in the FM-coupled bilayer, this transition is abrupt, which reduces the errors in reading [Figs. 4(f) and 4(g)].

Using CCM,[11,15] the equations of motion of the paired DWs with strong interlayer FM coupling were derived

$$\frac{2\alpha}{\Delta}\dot{q} + \dot{\varphi}_L + \dot{\varphi}_U = \frac{\pi\gamma_0 H_{SO} J(\cos\varphi_L + \cos\varphi_U)}{2} + 2\gamma_0 H_z, \quad (4)$$

$$\frac{\dot{q}}{\Delta} - \alpha\dot{\varphi}_L = \frac{\gamma_0\pi D\sin(\varphi_L)}{2\Delta\mu_0 M_s} + \frac{\gamma_0 N_x M_s\sin(2\varphi_L)}{2} + \frac{2\sigma\gamma_0\sin(\varphi_L-\varphi_U)}{\mu_0 M_s t_s} + \frac{\gamma_0\pi H_x\sin\varphi_L}{2} - \frac{\gamma_0 H_y\pi\cos\varphi_L}{2}, \quad (5)$$

$$\frac{\dot{q}}{\Delta} - \alpha\dot{\varphi}_U = \frac{\gamma_0\pi D\sin(\varphi_U)}{2\Delta\mu_0 M_s} + \frac{\gamma_0 N_x M_s\sin(2\varphi_U)}{2} - \frac{2\sigma\gamma_0\sin(\varphi_L-\varphi_U)}{\mu_0 M_s t_s} + \frac{\gamma_0\pi H_x\sin\varphi_U}{2} - \frac{\gamma_0 H_y\pi\cos\varphi_U}{2}. \quad (6)$$

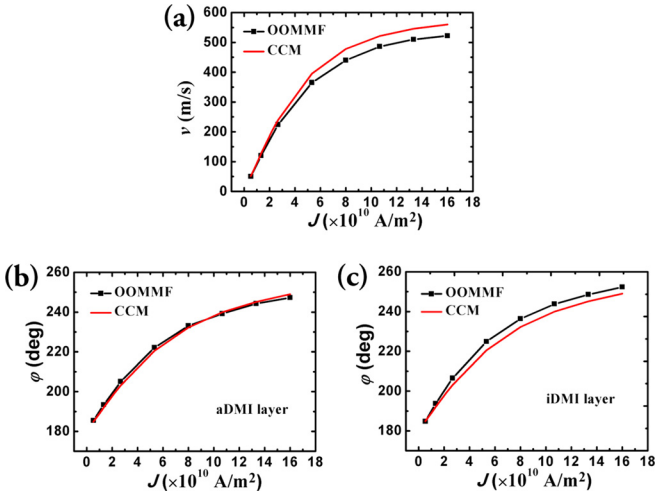

FIG. 5. (a) Velocity of the paired DWs, (b) azimuthal angle of the FM layer with aDMI, and (c) azimuthal angle of the FM layer with iDMI determined by micromagnetic simulation using OOMMF (black dots and lines) and CCM (red lines). D_x of both layers, σ, and w is -1.5 mJ/m^2, -0.06 mJ/m^2, and 100 nm, respectively.

Here, the collective coordinates q and φ_L and φ_U depict the central position of the coupled DWs and the azimuthal angles of magnetization in the central of the DWs of the lower and upper layers, respectively (Fig. 2). α, γ_0, μ_0, N_x, t_s, H_x, H_y, H_z, and H_{SO} are the Gilbert damping coefficient, the gyromagnetic ratio of an electron, the vacuum permeability, the demagnetization factor in the x-direction, the thickness of the NM layer, the x, y, and z components of the external magnetic field, and the SOT effective field, respectively. N_x and H_{SO} can be expressed as[12]

$$N_x = L_z \ln 2/\pi\Delta \quad (7)$$

and

$$H_{SO} = \mu_B\theta_{SH}J/\gamma_0 e M_s L_z, \quad (8)$$

where L_z, μ_B, and e are the thickness of the FM layer, the Bohr magneton, and the charge of electron, respectively.

Equations (4)–(6) were solved numerically using a fourth order Runge–Kutta algorithm (Fig. 5). The DW velocity and the azimuthal angles in both FM layers increase with the increasing J. The results of CCM agree well with that determined by OOMMF. The small difference between them is attributed to the boundary effect that was not considered in CCM.

In summary, the SOT-induced DW motion in the FM-coupled HM1/FM1/NM/FM2/HM2 multilayers was investigated numerically. The difference of DMIs (aDMI for the bottom HM/FM bilayer and iDMI for the upper one) resulted in the tilting of the two DWs toward opposite directions. When the interlayer exchange coupling was sufficiently strong, this tilting was effectively inhibited. As a result, the DW velocity was increased and the minimum allowed spacing between the neighboring DWs was reduced, which suggests the possibility of fabricating a racetrack memory with high reading speed, large storage density, and good readability.

See supplementary material for the DW velocity v, the DW magnetization orientation φ, and the DW tilting angle β

as a function of current density and DMI via the micromagnetic simulation (**S1**), for the influence of the external magnetic field along the *y* direction on the SOT-induced motion of the DW with the aDMI using the micromagnetic simulation (**S2**), for the SOT-induced motion of the DW with the aDMI using the collective coordinate methods (**S3**), and for the influence of the fieldlike torque on the motion of the paired DWs using the micromagnetic simulation (**S4**).

This work was supported by the National Natural Science Foundation of China (Grant Nos. 11574096 and 61674062) and Huazhong University of Science and Technology (No. 2017KFYXJJ037).

[1]S. S. P. Parkin, M. Hayashi, and L. Thomas, "Magnetic domain-wall racetrack memory," Science **320**, 190–194 (2008).
[2]S.-H. Yang and S. Parkin, "Novel domain wall dynamics in synthetic antiferromagnets," J. Phys.: Condens. Matter **29**, 303001 (2017).
[3]J. Sampaio, V. Cros, S. Rohart, A. Thiaville, and A. Fert, "Nucleation, stability and current-induced motion of isolated magnetic skyrmions in nanostructures," Nat. Nanotechnol. **8**, 839–844 (2013).
[4]S. Woo, K. Litzius, B. Krüger, M.-Y. Im, L. Caretta, K. Richter, M. Mann, A. Krone, R. M. Reeve, M. Weigand, P. Agrawal, I. Lemesh, M.-A. Mawass, P. Fischer, M. Kläui, and G. S. D. Beach, "Observation of room-temperature magnetic skyrmions and their current-driven dynamics in ultrathin metallic ferromagnets," Nat. Mater. **15**, 501 (2016).
[5]S. Emori, U. Bauer, S.-M. Ahn, E. Martinez, and G. S. D. Beach, "Current-driven dynamics of chiral ferromagnetic domain walls," Nat. Mater. **12**, 611–616 (2013).
[6]K.-S. Ryu, L. Thomas, S.-H. Yang, and S. Parkin, "Chiral spin torque at magnetic domain walls," Nat. Nanotechnol. **8**, 527–533 (2013).
[7]J. H. Franken, M. Herps, H. J. M. Swagten, and B. Koopmans, "Tunable chiral spin texture in magnetic domain-walls," Sci. Rep. **4**, 5248 (2014).
[8]S. Emori, E. Martinez, K.-J. Lee, H.-W. Lee, U. Bauer, S.-M. Ahn, P. Agrawal, D. C. Bono, and G. S. D. Beach, "Spin Hall torque magnetometry of Dzyaloshinskii domain walls," Phys. Rev. B **90**, 184427 (2014).
[9]A. Hrabec, N. A. Porter, A. Wells, M. J. Benitez, G. Burnell, S. McVitie, D. McGrouther, T. A. Moore, and C. H. Marrows, "Measuring and tailoring the Dzyaloshinskii-Moriya interaction in perpendicularly magnetized thin films," Phys. Rev. B **90**, 020402(R) (2014).
[10]K.-S. Ryu, L. Thomas, S.-H. Yang, and S. S. P. Parkin, "Current induced tilting of domain walls in high velocity motion along perpendicularly magnetized micron-sized Co/Ni/Co racetracks," Appl. Phys. Express **5**, 093006 (2012).
[11]O. Boulle, S. Rohart, L. D. Buda-Prejbeanu, E. Jué, I. M. Miron, S. Pizzini, J. Vogel, G. Gaudin, and A. Thiaville, "Domain wall tilting in the presence of the Dzyaloshinskii-Moriya interaction in out-of-plane magnetized magnetic nanotracks," Phys. Rev. Lett. **111**, 217203 (2013).
[12]E. Martinez, S. Emori, N. Perez, L. Torres, and G. S. D. Beach, "Current-driven dynamics of Dzyaloshinskii domain walls in the presence of in-plane fields: Full micromagnetic and one-dimensional analysis," J. Appl. Phys. **115**, 213909 (2014).
[13]J. Yun, D. Li, B. Cui, X. Guo, K. Wu, X. Zhang, Y. Wang, J. Mao, Y. Zuo, and L. Xi, "Current induced domain wall motion and tilting in Pt/Co/Ta structures with perpendicular magnetic anisotropy in the presence of the Dyzaloshinskii-Moriya interaction," J. Phys. D: Appl. Phys. **51**, 155001 (2018).
[14]I. Purnama, I. S. Kerk, G. J. Lim, and W. S. Lew, "Coupled Néel domain wall motion in sandwiched perpendicular magnetic anisotropy nanowires," Sci. Rep. **5**, 8754 (2015).
[15]S.-H. Yang, K.-S. Ryu, and S. Parkin, "Domain-wall velocities of up to $750\,\mathrm{m\,s^{-1}}$ driven by exchange-coupling torque in synthetic antiferromagnets," Nat. Nanotechnol. **10**, 221 (2015).
[16]Z. Yu, Y. Zhang, Z. Zhang, M. Cheng, Z. Lu, X. Yang, J. Shi, and R. Xiong, "Domain-wall motion at an ultrahigh speed driven by spin–orbit torque in synthetic antiferromagnets," Nanotechnology **29**, 175404 (2018).
[17]O. Alejos, V. Raposo, L. Sanchez-Tejerina, R. Tomasello, G. Finocchio, and E. Martinez, "Current-driven domain wall dynamics in ferromagnetic layers synthetically exchange coupled by a spacer: A micromagnetic study," J. Appl. Phys. **123**, 013901 (2018).
[18]A. K. Nayak, V. Kumar, T. Ma, P. Werner, E. Pippel, R. Sahoo, F. Damay, U. K. Rößler, C. Felser, and S. S. P. Parkin, "Magnetic antiskyrmions above room temperature in tetragonal Heusler materials," Nature **548**, 561 (2017).
[19]M. Hoffmann, B. Zimmermann, G. P. Müller, D. Schürhoff, N. S. Kiselev, C. Melcher, and S. Blüge, "Antiskyrmions stabilized at interfaces by anisotropic Dzyaloshinskii-Moriya interactions," Nat. Commun **8**, 308 (2017).
[20]L. Camosi, S. Rohart, O. Fruchart, S. Pizzini, M. Belmeguenai, Y. Roussigné, A. Stashkevich, S. M. Cherif, L. Ranno, M. Santis, and J. Vogel, "Anisotropic Dzyaloshinskii-Moriya interaction in ultrathin epitaxial Au/Co/W(110)," Phys. Rev. B **95**, 214422 (2017).
[21]S. Huang, C. Zhou, G. Chen, H. Shen, A. K. Schmid, K. Liu, and Y. Wu, "Stabilization and current-induced motion of antiskyrmion in the presence of anisotropic Dzyaloshinskii-Moriya interaction," Phys. Rev. B **96**, 144412 (2017).
[22]A. Samardak, A. Kolesnikov, M. Stebliy, L. Chebotkevich, A. Sadovnikov, S. Nikitov, A. Talapatra, J. Mohanty, and A. Ognev, "Enhanced interfacial Dzyaloshinskii-Moriya interaction and isolated skyrmions in the inversion-symmetry-broken Ru/Co/W/Ru films," Appl. Phys. Lett. **112**, 192406 (2018).
[23]S. Krishnia, P. Sethi, W. L. Gan, F. N. Kholid, I. Purnama, M. Ramu, T. S. Herng, J. Ding, and W. S. Lew, "Role of RKKY torque on domainwall motion in synthetic antiferromagnetic nanowires with opposite spin Hall angles," Sci. Rep. **7**, 11715 (2017).
[24]S. Rohart and A. Thiaville, "Skyrmion confinement in ultrathin film nanostructures in the presence of Dzyaloshinskii-Moriya interaction," Phys. Rev. B **88**, 184422 (2013).
[25]Y. Zhou and M. Ezawa, "A reversible conversion between a skyrmion and a domain-wall pair in a junction geometry," Nat. Commun. **5**, 4652 (2014).
[26]Y. Zhang, S. Luo, X. Yang, and C. Yang, "Spin-orbit-torque-induced magnetic domain wall motion in Ta/CoFe nanowires with sloped perpendicular magnetic anisotropy," Sci. Rep. **7**, 2047 (2017).
[27]F. B. Hagedorn, "Dynamic conversion during magnetic bubble domain wall motion," J. Appl. Phys. **45**, 3129 (1974).